modelling

MDPI

Article

Multiscale Modeling of Thermoplastic Matrix Composites for Cryogenic Hydrogen Storage Applications

Brett A. Bednarcyk *, Brandon L. Hearley and Evan J. Pineda

Multiscale and Multiphysics Modeling Branch, NASA Glenn Research Center, Cleveland, OH 44135, USA
* Correspondence: brett.a.bednarcyk@nasa.gov

Abstract

The performance of thermoplastic matrix composites for linerless Type V cryotanks is evaluated via a partially coupled, multiscale computational workflow with the objective of assessing the choice of thermoplastic matrix material under realistic conditions. Atomistic molecular dynamics simulations provide temperature-dependent stiffness, thermal expansion, and yield strength data for six candidate thermoplastics. These inputs feed into a recursive micromechanics model that simulates a stress-free cooldown to liquid hydrogen temperature, followed by biaxial hoop to longitudinal loading representative of a cylindrical tank's acreage. Progressive damage analyses predict the onset of matrix microcracking and ultimate burst behavior across four industry-relevant layups. Results highlight that $[55/5/-55/-5]$ Double-Double or $[0/\pm30/\pm60]_s$ layup architectures with low-melt poly(aryl ether ketone) or poly(ether ketone ketone) matrices deliver superior microcrack resistance, illustrating the power of this framework to guide material and layup selection for leak-resistant thermoplastic composite cryotanks.

Keywords: thermoplastic composites; cryotanks; modeling; micromechanics; pressure vessels; molecular dynamics; hydrogen tanks

check for updates

Academic Editors: Wei Gao and Alfredo Cuzzocrea

Received: 4 September 2025
Revised: 26 September 2025
Accepted: 30 September 2025
Published: 20 November 2025

Citation: Bednarcyk, B.A.; Hearley, B.L.; Pineda, E.J. Multiscale Modeling of Thermoplastic Matrix Composites for Cryogenic Hydrogen Storage Applications. *Modelling* **2025**, *6*, 151. https://doi.org/10.3390/modelling6040151

Copyright: © 2025 by the authors. Licensee MDPI, Basel, Switzerland. This article is an open access article distributed under the terms and conditions of the Creative Commons Attribution (CC BY) license (https://creativecommons.org/licenses/by/4.0/).

1. Introduction

Hydrogen fuel storage remains a central challenge in enabling efficient and sustainable aerospace propulsion systems. Among the most demanding applications is the containment of cryogenic hydrogen in linerless composite pressure vessels. These Type V (see Figure 1) cryotanks require materials capable of maintaining structural integrity, without significant leakage, at liquid hydrogen temperatures (−253 °C), while withstanding internal pressures. While challenging to realize, the weight savings associated with linerless composite tanks continue to be a compelling benefit driving current development efforts.

Thermoplastic matrix composites (TPCs) have emerged as strong candidates for cryogenic composite structures, particularly cryotanks, due to their inherent toughness, chemical resistance, and advantageous processing characteristics. A growing body of studies in the literature has reinforced their suitability for such applications, including multiple recent review papers. Saha and Sullivan [1] reported that thermoplastics such as poly(ether ether ketone) (PEEK) and poly(ether ketone ketone) (PEKK) exhibit gas permeabilities several orders of magnitude lower at cryogenic temperatures compared to room temperature, attributed to the closing of gaps at the fiber/matrix interface and a reduced tendency for microcracking relative to thermoset epoxies. Nachtane et al. [2] agreed, identifying thermoplastics as a promising technology for future cryotank designs. Similarly, Chen et al. [3] highlighted the superior fracture toughness and microcrack resistance of

high-performance thermoplastics at cryogenic temperatures, though they also noted that processing requirements and higher manufacturing costs had historically limited broader adoption. Sápi and Butler [4] further supported these findings, concluding that thermoplastic composites demonstrate better retention of mechanical properties, such as strength, modulus, and impact resistance, compared to thermosets under cryogenic conditions, largely due to enhanced fiber/matrix bonding and reduced microcracking. Hohe et al. [5] likewise emphasized the potential of carbon fiber-reinforced thermoplastics, citing their superior toughness and microcrack resistance compared to thermosets as key advantages for cryotank applications.

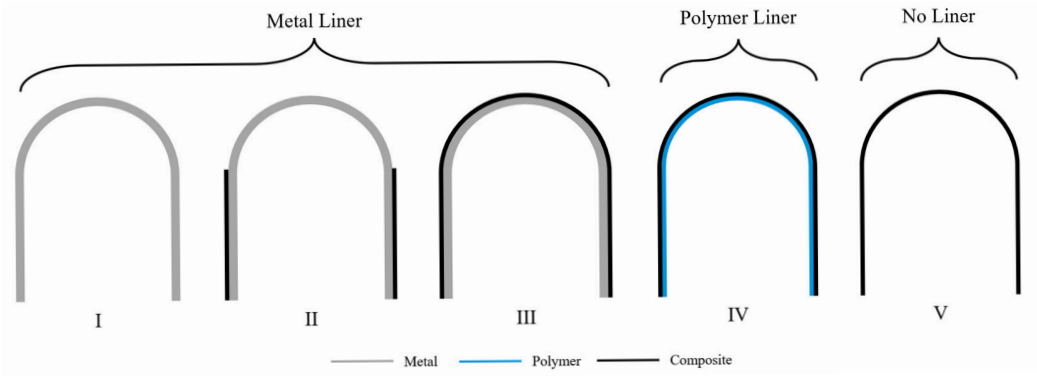

Figure 1. Common types of pressure vessels and their standard numeric designations.

Numerous other studies have evaluated the cryogenic performance of thermoplastic matrix composites, reflecting a sustained interest spanning over two decades. Early work by Wang and Sun [6] highlighted the development of residual stresses during cooldown in PEEK composites, underscoring critical design considerations for cryogenic use. Whitley and Gates [7] further validated the structural viability of thermoplastic composites at cryogenic temperatures through combined experimental and simulation approaches. Building on this foundation, Grogan et al. [8] identified microcrack formation in cryogenically cycled carbon/PEEK laminates, providing detailed damage characterization that revealed the superior toughness and damage tolerance of thermoplastics compared to thermosets. Their subsequent study [9] connected laminate design parameters to hydrogen permeability in tape-laid thermoplastic tanks, emphasizing the importance of microstructural control in preserving structural integrity and minimizing leakage. Complementing these experimental insights, Grogan et al. [10,11] developed advanced XFEM and cohesive zone modeling frameworks to simulate fatigue delamination and microcracking, capturing the complex crack propagation and permeability behavior intrinsic to thermoplastic composites. This focus on C/PEEK arose from thermoplastics' enhanced fracture toughness, better impact resistance, and improved thermal performance at cryogenic temperatures, qualities essential for demanding applications such as cryotanks. At this time, Comer et al. [12] demonstrated that laser-assisted tape placement can manufacture carbon/PEEK laminates with minimal cryogenic strength degradation. Flanagan [13] also corroborated the low permeability and structural reliability of carbon/PEEK composites for space-based cryogenic storage systems, underscoring their growing adoption in advanced cryogenic applications.

More recent investigations have continued to build on these findings; for example, Schlothauer et al. [14] showed that tailoring microstructure and morphology can significantly enhance transverse performance under cryogenic conditions. Nikonovich et al. [15] confirmed that PEEK-based composites maintain beneficial thermal and mechanical properties at low temperatures, and Pourahmadi et al. [16] employed micromechanical modeling to accurately predict stiffness in AFP-fabricated carbon/PEEK composites relevant to cryogenic environments. Additionally, Wang et al. [17] investigated the sealing behavior

of thermoplastics, highlighting the influence of strain rate and temperature sensitivity on performance.

While not specifically focused on TPCs, the highly relevant foundational work on cryogenic composites by Roy and Benjamin [18] should be mentioned. This work created a unique model to predict permeation by deriving expressions for delaminated crack opening displacement and applying Darcy's law to model gas flow through networks formed by transverse matrix cracks and inter-ply delaminations. Building on this, Nair and Roy [19] extended the model to generic laminate configurations, introducing the concept of "stitch cracks" observed in off-axis plies that do not necessarily span the entire ply width. A number of studies since then have utilized the approach introduced in these papers.

While the literature demonstrates the potential for TPCs for cryotanks, there is a clear need for advanced design tools capable of evaluating the performance of composite cryotanks across thermoplastic matrix systems and laminate configurations under realistic service conditions. These tools must capture the complex interactions among material behavior, damage evolution, and structural response across the temperatures encountered by in-service cryotanks. Accurate evaluation requires reliable input data, yet comprehensive thermal and mechanical characterization of thermoplastic composites across this full temperature range remains limited. To address this gap, this study employs molecular dynamics (MD) simulations to predict consistent, temperature-dependent properties of thermoplastic matrices. This approach enables the generation of reliable, fine-scale data where experimental measurements are challenging or impractical, providing the foundational material inputs necessary for robust multiscale modeling and performance prediction of the cryogenic composite structures.

The nano-scale MD thermoplastic property predictions are used as input to a multiscale micromechanics model considering both the micro (fiber/matrix) and macro (ply layup) scales in a coupled manner. This enables the capture of residual stresses at the fiber/matrix constituent scale, which then influences the progressive damage predictions during the applied mechanical loading. The result is a realistic evaluation of promising thermoplastic matrix materials for use in linerless TPC cryogenic tanks.

2. Multiscale Micromechanics Model

The multiscale modeling approach for the TPCs is illustrated in Figure 2. At the lowest (nano) length scale, MD simulations were conducted using the LAMMPS software (LAMMPS stable release 29 September 2021) [20] to obtain the properties of each neat thermoplastic material at 27 °C, −183 °C, and −253 °C. These properties were then used as input for the matrix in a micromechanics analysis for each ply, and these micromechanics simulations were coupled within a global, macro-scale micromechanics model representing the ply layup. The AS4 carbon fiber was considered in this study. It was treated as temperature-independent and transversely isotropic, with the properties given in Table 1.

Table 1. AS4 carbon fiber properties [21].

Material	E_{11} (GPa)	E_{22} (GPa)	ν_{12}	ν_{23}	G_{12} (GPa)	CTE_{11} (10^{-6}/°C)	CTE_{22} (10^{-6}/°C)	Failure Strain
AS4 Carbon Fiber	225	15	0.2	0.0714 *	15	−0.5	15	0.01488

* Ref. [21] provided G_{23}, from which, assuming transverse isotropy, ν_{23} was calculated.

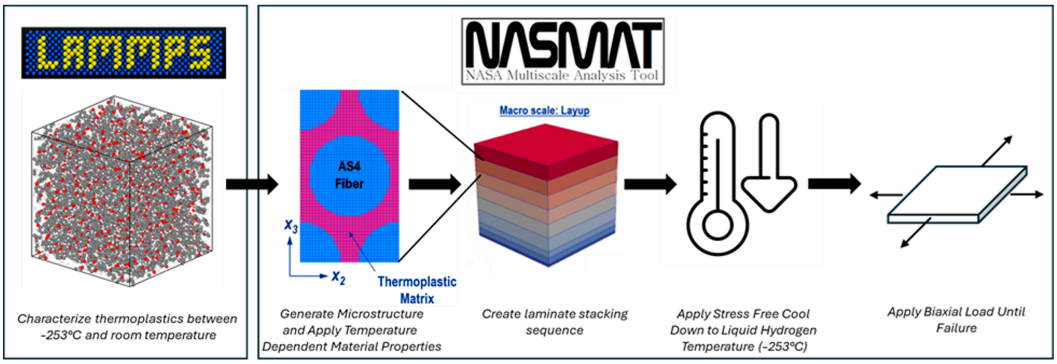

Figure 2. Multiscale analysis used for the TPC composites. The LAMMPS MD simulations are uncoupled from the micromechanics, but the NASMAT macroscale layup RUC and the microscale hexagonally packed RUC are fully coupled during the stress-free cool down and the progressive damage simulations.

As shown in Figure 2, at the micro scale, a repeating unit cell (RUC) with hexagonally packed fibers was represented (32×56 subvolumes with a fiber volume fraction of 0.603). For the macroscale, the layup RUC representation is essentially 1-D, with the ply materials stacked in the Z-direction. It should be noted that, while the RUC accurately represents the material behavior of the layup, it is not capable of predicting bending as would a plate theory. That is, because it is repeated infinitely, the RUC automatically achieves homogenization, and no bending-extension coupling can be captured.

Four layups that are realistic for cryotanks have been considered. These are (1) a quasi-isotropic $[0/\pm45/90]_s$ layup, (2) a hard layup $[0_4/\pm45/90_2]_s$ with a higher percentage of zeros, (3) a $[0/\pm30/\pm60]_s$ layup, and (4) a $[55/5/-55/-5]$ Double-Double layup. Note that the 0-direction refers to the hoop direction in this study. Double-Double is a family of laminates developed by Tsai [22,23] that can offer performance and manufacturability advantages. Double-Double layups involve two $\pm$ angles in a four-ply repeating block, such as $[\Phi/\Psi/-\Phi/-\Psi]_n$, where the ordering of the plies within a given repeating block defines the Type. Herein, one particular Double-Double layup, with ply ordering considered as Type II [22], has been considered with a 5° angle (close to the hoop direction) and an intermediate 55° angle to provide some stiffness and strength in the direction that would correspond to the longitudinal tank direction. Note that the chosen Double-Double layup, as well as the other layups considered, have not been optimized for the current cryotank application.

2.1. Molecular Dynamics Modeling of Neat Thermoplastics

Molecular dynamics (MD) simulations were used to predict key physical, thermal, and mechanical properties of six high-performance thermoplastic polymers: PEEK, Elium, LM-PAEK, PEKK, poly(ether imide) (PEI), and polyimide, across a wide temperature range down to –253 °C, relevant for liquid hydrogen storage. These MD simulations are described in detail by Bamane et al. [24] and are briefly summarized here. Using the LAMMPS simulation package and the IFF-R force field, atomistic models of the amorphous thermoplastics were built, equilibrated, polymerized (when applicable), and subjected to controlled cooling and mechanical deformation protocols. The simulations yielded temperature-dependent predictions of mass density, free volume, thermal shrinkage, Young's modulus, yield strength, Poisson's ratio, and the coefficient of thermal expansion (CTE). These properties were determined at 27 °C, −183 °C (liquid oxygen), and −253 °C (liquid hydrogen), providing consistent input for cryogenic composite design. The thermoplastic systems, especially PEEK, LM-PAEK, and polyimide, were found to exhibit low shrinkage, stable

stiffness, and favorable CTE at cryogenic temperatures, supporting their suitability as matrix candidates in composite cryotank applications where experimental characterization is challenging. The neat thermoplastic properties are provided in Table 2. Bamane et al. [24] provide some validation comparisons to experimental data for the MD-predicted density, Young's modulus, and yield strength.

Table 2. Neat thermoplastic properties predicted using MD [24].

Material	Temperature (°C)	Density (kg/m^3)	E (GPa)	ν	G (GPa)	CTE (10^{-6}/°C)	Yield Strength (MPa)
PEEK	−253	1310	4.35	0.404	1.55	54.3	166
	−183	1300	3.78	0.411	1.34	55.4	133
	27	1250	2.62	0.431	0.915	67.7	81.3
Elium	−253	1240	7.32	0.324	2.76	73.9	265
	−183	1220	6.44	0.333	2.42	75.7	223
	27	1170	3.72	0.385	1.34	73.6	123
LM-PAEK	−253	1300	3.47	0.391	1.25	45.1	171
	−183	1290	3.24	0.398	1.16	45.3	128
	27	1250	2.43	0.419	0.856	60.4	90.4
PEKK	−253	1300	3.29	0.341	1.23	48.1	138
	−183	1280	2.99	0.343	1.11	46.2	124
	27	1240	2.04	0.313	0.779	52.6	57.6
PEI	−253	1330	4.42	0.391	1.59	47.9	132
	−183	1310	3.68	0.409	1.31	47.3	114
	27	1270	2.48	0.413	0.876	62.8	64.6
Poly imide	−253	1320	4.80	0.375	1.75	47.1	168
	−183	1310	4.35	0.389	1.56	52.3	132
	27	1240	2.64	0.397	0.944	61.3	95.5

It should be emphasized that all of the neat thermoplastics were modeled as amorphous, whereas it is well-known that PEEK, LM-PAEK, and PEKK are semi-crystalline. As such, the predictions involving these materials should be considered estimates. Future work will consider the semi-crystalline nature of these thermoplastics via additional, lower length scales in the model to capture the crystalline phase and its microstructure. See [25,26] for examples of this approach.

2.2. Multiscale Recursive Micromechanics

In multiscale recursive micromechanics (MsRM), synergistic material modeling is achieved by linking scales such that the homogenized response of a representative unit cell (RUC) at scale i becomes the local input for a subvolume at the next finer scale, $i + 1$. This coupling, illustrated conceptually in Figure 3, may include coordinate transformations to reconcile differences in orientation between scales. Upward and downward transfer of information is facilitated through homogenization and localization, respectively. Within the NASMAT framework, a flexible selection of micromechanics models, ranging from Mori-Tanaka and the Generalized Method of Cells (GMC) to the High-Fidelity Generalized Method of Cells (HFGMC) and full finite element, can be applied at any number of recursive scales. While Figure 3 shows two branches for clarity, the framework supports arbitrarily deep hierarchies to capture the full multiscale nature of advanced composite materials.

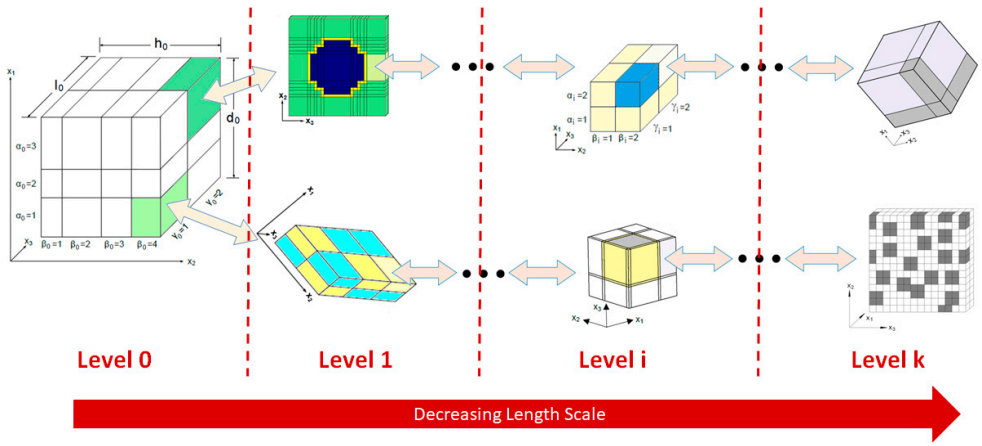

Figure 3. MsRM integrated hierarchy linking RUCs and subcells across an arbitrary number of length scales.

Each micromechanics model computes a strain concentration tensor, $\mathbf{A}_i^{(\alpha_i)}$, which maps the global strain at level i, $\bar{\boldsymbol{\varepsilon}}_i$, to the local strain in subvolume, α_i,

$$\boldsymbol{\varepsilon}_i^{(\alpha_i)} = \mathbf{A}_i^{(\alpha_i)} \bar{\boldsymbol{\varepsilon}}_i \tag{1}$$

The local stress components are computed using material-specific constitutive laws:

$$\boldsymbol{\sigma}_i^{(\alpha_i)} = \mathbf{C}_i^{(\alpha_i)} \boldsymbol{\varepsilon}_i^{(\alpha_i)} \tag{2}$$

where $\mathbf{C}_i^{(\alpha_i)}$ is the local material stiffness tensor for a given subvolume. Global averages for the stresses are obtained by volume-weighted sums across all subvolumes:

$$\bar{\boldsymbol{\sigma}}_i = \sum_{\alpha_i=1}^{N_{\alpha_i}} v_{\alpha_i} \boldsymbol{\sigma}_i^{(\alpha_i)} \tag{3}$$

with v_{α_i} denoting the relative volume fraction of each subvolume. The effective (homogenized) stiffness and thermal conductivity tensors for the RUC are then computed as:

$$\mathbf{C}_i^{*} = \sum_{\alpha_i=1}^{N_{\alpha_i}} v_{\alpha_i} \mathbf{C}_i^{(\alpha_i)} \mathbf{A}_i^{(\alpha_i)} \tag{4}$$

To propagate material behavior between scales, homogenized properties from level $i+1$ are mapped to level i using appropriate transformation tensors,

$$\mathbf{C}_i^{(\alpha_i)} = \mathbf{T}_4^{i+1} \, \mathbf{C}_{i+1}^{*}, \qquad i = 0, \ldots, k-1 \tag{5}$$

$$\bar{\boldsymbol{\varepsilon}}_i = \left(\mathbf{T}_2^{i}\right)^{-1} \boldsymbol{\varepsilon}_{i-1}^{(\alpha_{i-1})}, \qquad i = 1, \ldots, k \tag{6}$$

where $\mathbf{T}_2^i$ and $\mathbf{T}_4^i$ are the appropriate second and fourth order coordinate transformation tensors if the two linked RUCs are oriented differently in space.

Herein, the well-documented HFGMC micromechanics theory [27,28] was used to predict the behavior of the TPCs. Summarizing, this semi-analytical approach analyzes a repeating unit cell composed of rectangular parallelepiped subvolumes. Assuming a quadratic displacement field in each subvolume, equilibrium is enforced within each subvolume, and continuity between subvolumes, as well as periodicity, are enforced via the surface-averaged tractions and displacements. This results in a system of linear algebraic

equations that can be solved to obtain the effective (homogenized) properties of the RUC, as well as the local fields in each subvolume via the strain concentration tensor, see Equation (1). Both doubly periodic (considering a 2-D RUC) and triply periodic (considering a 3-D RUC) formulations of the HFGMC theory are available [27,28]. The HFGMC theory and MsRM have been implemented in the NASA Multiscale Analysis Tool (NASMAT) [29,30], which includes nonlinear effects such as progressive damage and plasticity. The progressive damage simulations presented here are based on a simple subvolume elimination approach. The simulation applies the loading incrementally, and once a subvolume (thermoplastic or fiber) reaches the specified material strength (or failure strain), its stiffness is instantaneously reduced to a low value. Recall that, for the thermoplastic materials, the yield strength predicted by the MD simulations was used as the material strength. For the AS4 fiber, only longitudinal (fiber-direction) failure was considered (using the max strain criterion, see Table 1). It is well-known that simple subvolume elimination, while very numerically stable, leads to discretization-dependent results for methods that are able to capture localization (such as HFGMC and the finite element method) [28]. As such, in the present study, the micro-scale subvolume discretization was kept fixed to keep the results consistent with each other. Future work will employ energy-based progressive failure methods incorporating a length scale to make the results more discretization objective and quantitatively predictive.

3. Results and Discussion

The progressive damage simulations began with a stress-free thermal cooldown from 25 °C to −253 °C, followed by mechanical loading under a 2:1 hoop-to-longitudinal stress ratio, replicating the acreage service conditions in a cylindrical cryotank (Figure 4). This loading history induces thermal stresses due to CTE mismatch, both between the fiber and matrix and among the plies, setting the stage for subsequent matrix microcracking.

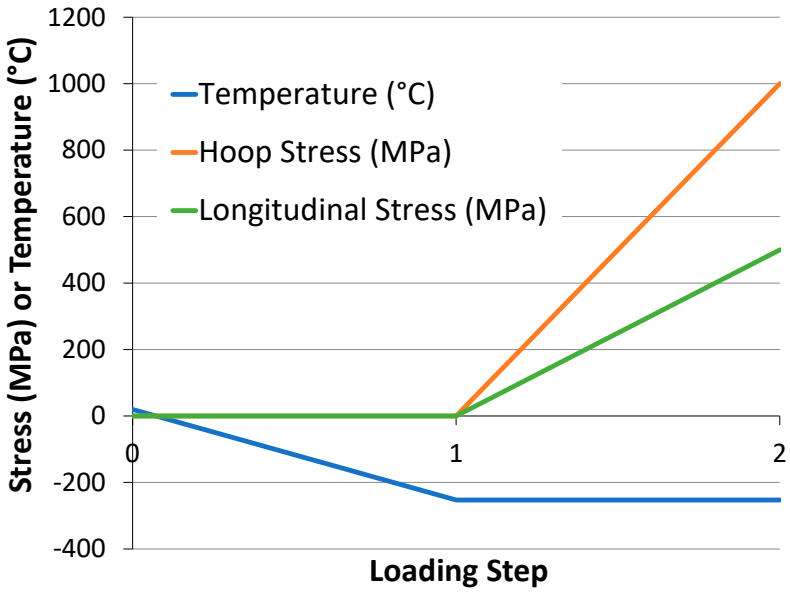

Figure 4. Loading history applied to the TPC layup. A stress-free cooldown from room temperature to −253 °C, followed by mechanical loading at a 2:1 ratio of hoop to longitudinal stress.

Figure 5 presents the hoop stress–hoop strain responses for each of the four layups, quasi-isotropic $[0/\pm45/90]_s$, hard $[0_4/\pm45/90_2]_s$, $[0/\pm30/\pm60]_s$, and the Double-Double configuration, and the six thermoplastic matrices. In all cases, the onset of matrix damage manifests as sudden strain jumps under stress control, serving as a proxy for microcrack initiation and, by extension, potential permeability. While the ultimate burst stress (associated

with fiber failure) was similar across materials and layups, the predicted damage initiation stresses varied widely. Notably, the PEEK and PEI matrix composites exhibited microcracking during cooldown, prior to any mechanical loading, indicating poor cryogenic performance for these thermoplastic systems compared to the others.

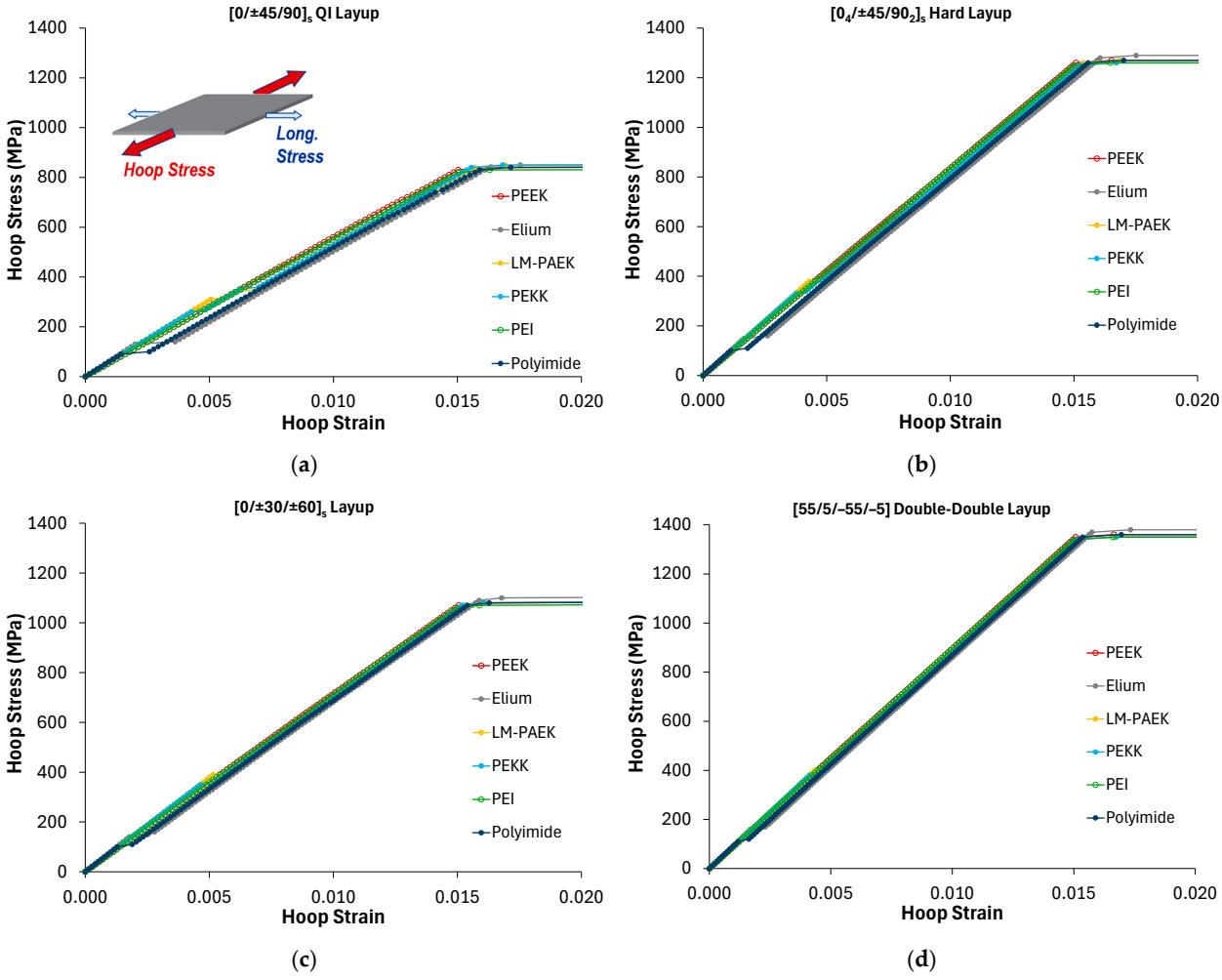

Figure 5. Progressive damage simulations for the four layups, showing the hoop stress vs. hoop strain response. (**a**) Quasi-isotropic (QI) $[0/\pm45/90]_s$. (**b**) Hard layup $[0_4/\pm45/90_2]_s$. (**c**) $[0/\pm30/\pm60]_s$ layup. (**d**) Double-Double layup $[55/5/-55/-5]$.

A clearer comparison of matrix performance is provided in Figure 6, which plots the composite hoop stress at first microcrack initiation for each combination of layup and thermoplastic matrix. Across all four layups, the composites with PEEK and PEI matrices exhibited microcrack initiation during the cooldown, prior to application of any biaxial mechanical loading. Microcracking occurred earlier in the PEI matrix composites (at −191 to −198 °C) compared to the PEEK matrix composites (at −226 to −233 °C). The $[55/5/-55/-5]$ Double-Double layup generally performed the best among the layups in terms of damage-initiation stress. For LM-PAEK and PEKK matrices, the ordering of the layups was consistent, with the $[0/\pm30/\pm60]_s$ performing second best, followed by the hard and quasi-isotropic (QI) layups. This is generally expected as the quasi-isotropic layup has only 25% of the plies in the more highly loaded hoop direction, whereas the other three layups are purposely biased toward hoop-direction reinforcement. For Elium, the trend was different, with the hard configuration performing marginally better than the $[0/\pm30/\pm60]_s$. Recall that these layup candidates are representative and not

truly optimized for the cryotank application. These results do, however, imply that if layup optimization were performed, it should be done for each layup and matrix material combination independently, as Figure 6 shows that different laminates perform better when paired with certain matrix materials.

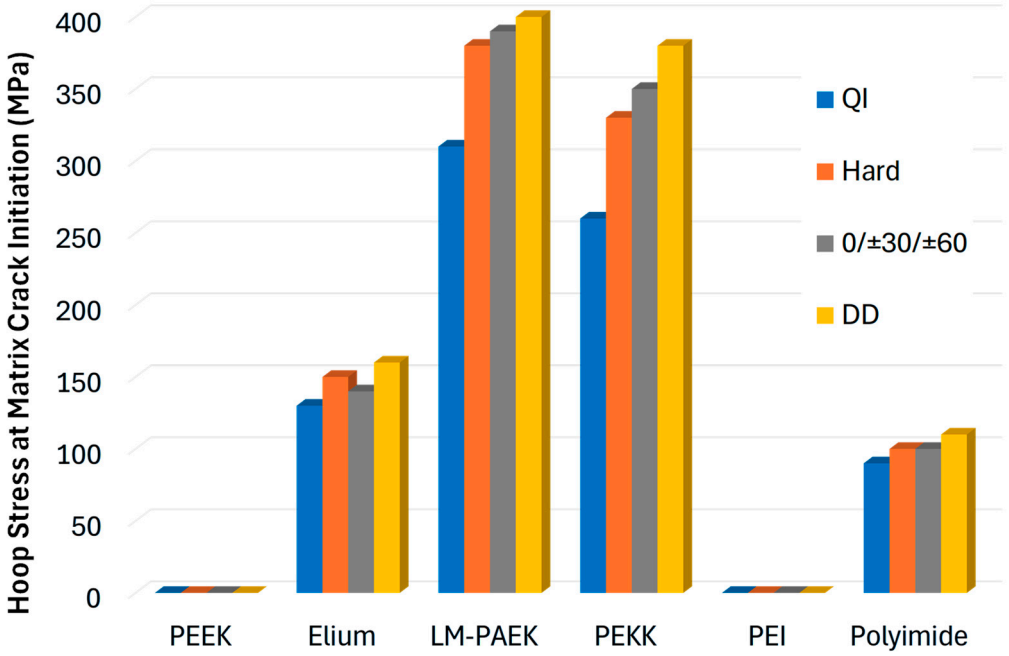

Figure 6. Predicted stress for initiation of matrix cracking in the TPC layups. PEI exhibited matrix cracking during the stress-free cooldown.

Among the thermoplastic matrices, LM-PAEK and PEKK stood out, achieving the greatest resistance to initial cracking under combined thermal and mechanical loading for all layups considered. Note that predicting actual permeability is beyond the scope of this study. This would require a 3D model to capture the cracking path (c.f., refs. [11,18]). Also, the simple, brittle subvolume elimination damage model does not account for material toughness. Use of a more advanced energy-based model would improve the fidelity of the performance predictions (but would require material toughness data as input). As mentioned previously, the results presented herein should be considered as representative and likely lower bounds on the TPC performance because the properties of the thermoplastic matrices were obtained from MD simulations treating them as purely amorphous, rather than semi-crystalline.

Detailed damage patterns for the two extremes, AS4/PEI (worst performing) and AS4/LM PAEK (best performing), in the $[0/\pm30/\pm60]_s$ layup are compared in Figures 7–9. During cooldown (Figure 7), PEI shows extensive microcracks emerging near −198 °C, whereas AS4/LM PAEK remains undamaged. Under the subsequent mechanical loading (Figure 8), AS4/PEI exhibits some continued damage propagation, while the AS4/LM PAEK microcracking is first seen only as the hoop stress approaches 400 MPa. At final failure (Figure 9), both composites "burst" when fiber strength is exceeded in the 0° plies, confirming that matrix toughness governs early damage but that fiber properties control ultimate burst.

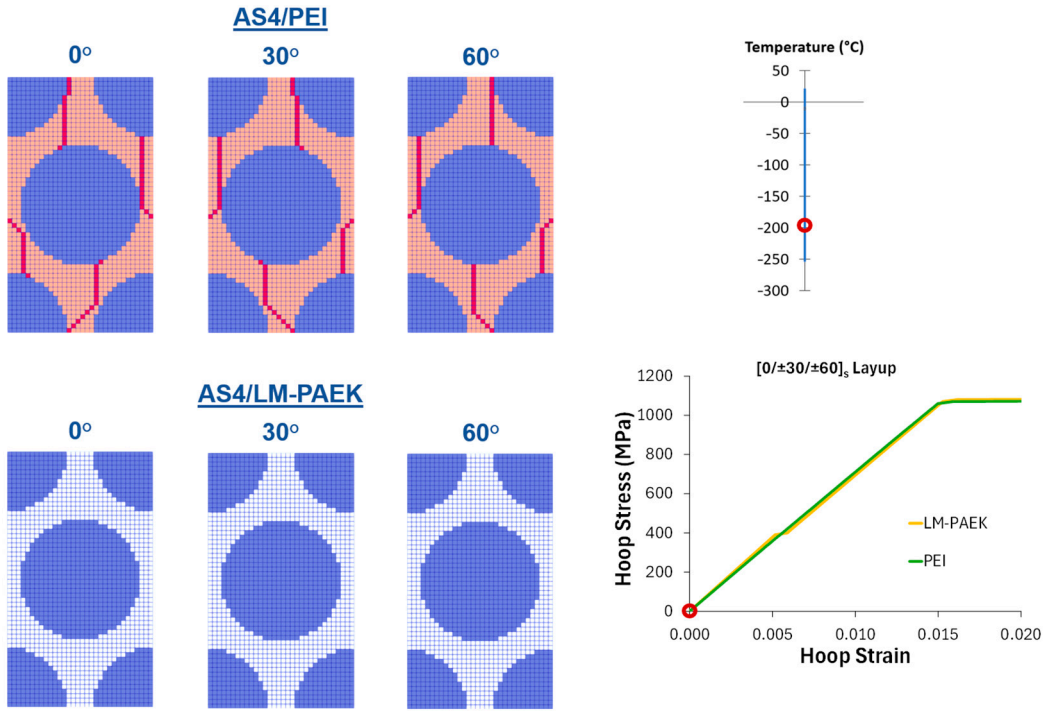

Figure 7. Snapshot comparison of the AS4/PEI and AS4/LM-PAEK damage patterns for the $[0/\pm30/\pm60]_s$ layup, per ply, during the cooldown. The red circles in the figures on the right indicate the applicable point in the simulation.

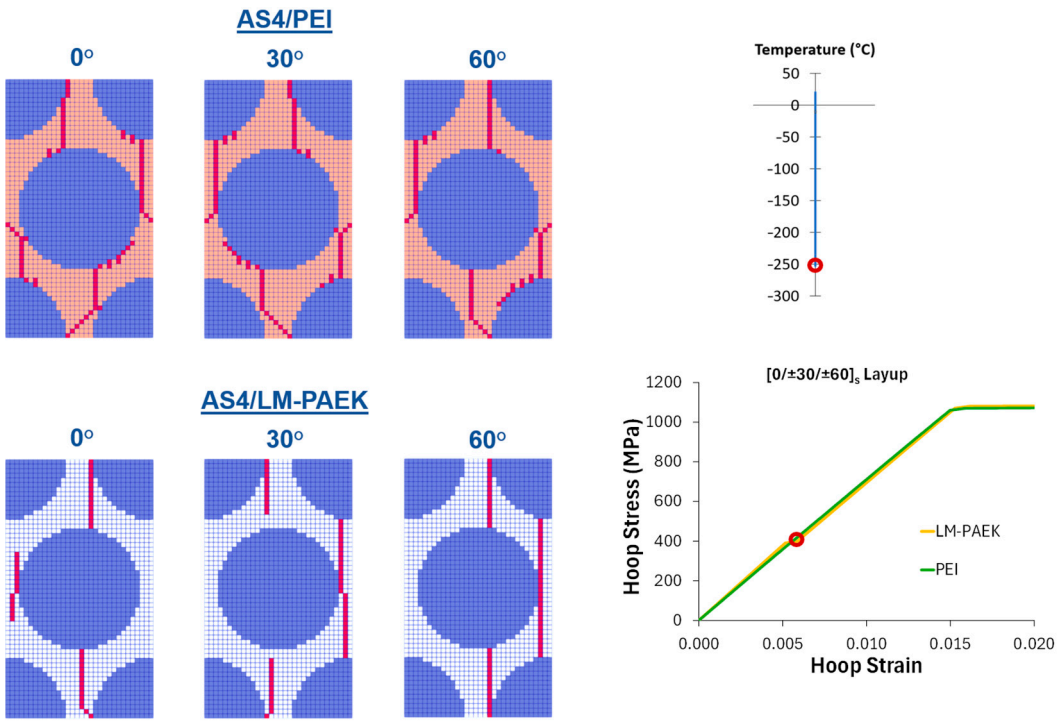

Figure 8. Snapshot comparison of the AS4/PEI and AS4/LM-PAEK damage patterns for the $[0/\pm30/\pm60]_s$ layup, per ply, during the mechanical loading. The red circles in the figures on the right indicate the applicable point in the simulation.

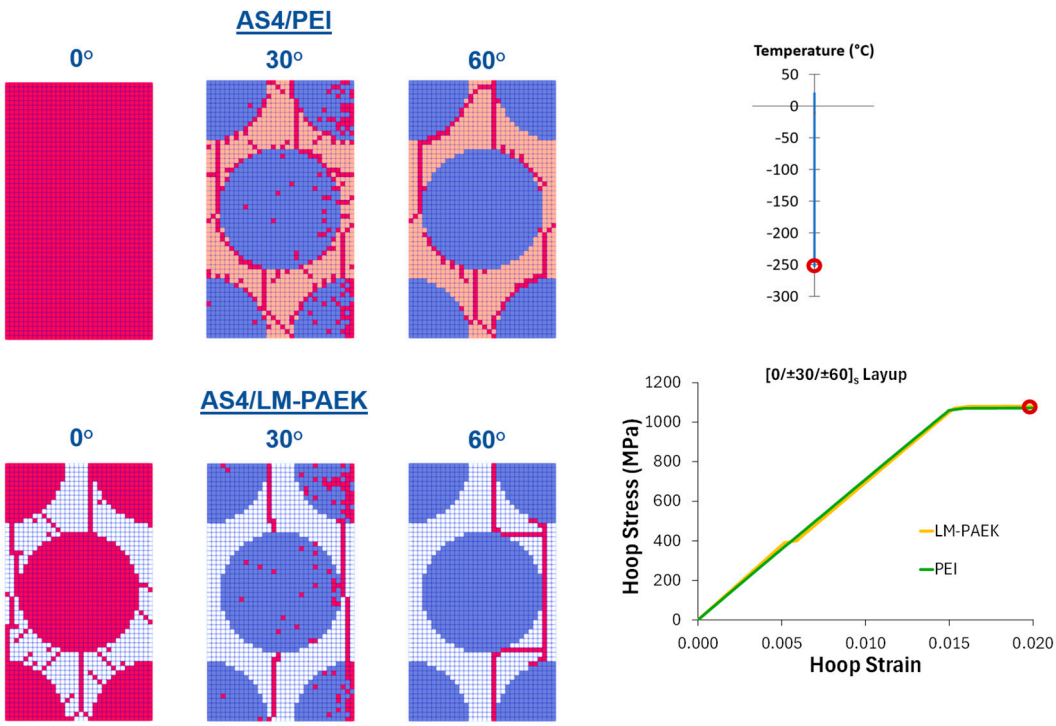

Figure 9. Snapshot comparison of the AS4/PEI and AS4/LM-PAEK damage patterns for the $[0/\pm30/\pm60]_s$ layup, per ply, at the end of the simulation.

In an attempt to tie the performance of the TPCs back to the thermoplastic matrix properties provided by MD, Figure 10 shows the thermoplastic Young's modulus times CTE vs. yield stress for the six thermoplastics at the three temperatures (see Table 2). The Young's modulus times CTE ($E \cdot \alpha$) drives the thermal stresses from mismatch with the fiber (since the fiber has a negative longitudinal CTE). The yield stress, which is used as the matrix strength in the progressive damage simulations, provides the resistance to the thermal stresses and the applied mechanical stresses. As such, high yield stress and low $E \cdot \alpha$ would indicate better expected performance, corresponding to the lower right of the plot in Figure 10. Clearly, Elium is an outlier, with the highest strengths and the highest $E \cdot \alpha$. This material had mid-range performance in Figure 6. The best performing thermoplastics, LM-PAEK and PEKK, have the lowest $E \cdot \alpha$, with strengths reasonably close to the other thermoplastics (aside from Elium). PEKK's strength at the lowest temperature (furthest point to the right in its curve) is quite a bit lower compared to LM-PAEK, and even PEEK and polyimide, but it has a much lower $E \cdot \alpha$ compared to these two lower-performing thermoplastics. Examining PEI, which, recall, had the worst performance of all the thermoplastics studied, it has the lowest strength at -253 °C (furthest point to the right in its curve), and it also has a significant jump in $E \cdot \alpha$ from -183 to -253 °C. However, given its poor performance, with TPC matrix microcracking during the cooldown, one might expect it to appear further from the other thermoplastics in the plot shown in Figure 5. The PEEK TPC also exhibited matrix microcracking during the cooldown, yet it is close to polyimide in Figure 5. Obviously, in the multiscale thermo-mechanical micromechanics simulations of the layup and the microstructure, there are complex, multiaxial interactions occurring that cannot be gleaned from a simple plot of the matrix input properties.

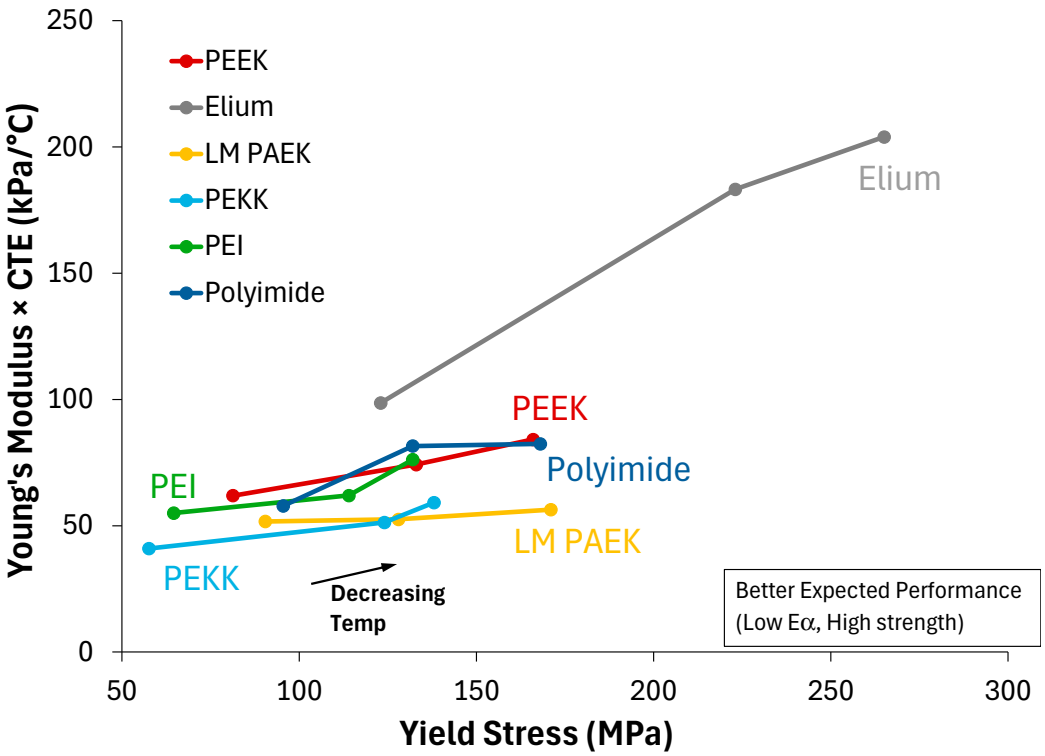

Figure 10. Plots of the Young's modulus times CTE vs. yield stress for the six thermoplastics at the three temperatures.

To further frame the presented results and provide evidence of their validity, predictions were made for a unidirectional AS4/PEEK composite at room temperature using the same 0.603 fiber volume fraction RUC employed within the layup plies (see Figure 2). To compare with test data from the literature, in which the PEEK matrix is typically semi-crystalline, estimates of the PEEK matrix properties as a function of crystallinity percentage (by volume) were first performed. Towards this end, the empirical equations presented by Talbott et al. [31], which provide the Young's modulus, tensile strength, and shear strength of neat PEEK as a function of crystallinity, were employed. For consistency with the neat PEEK properties employed herein (see Table 2), which, recall, represent fully amorphous PEEK, the Talbott et al. [31] equations were used to determine the percentage change in the neat PEEK properties as a function of crystallinity. These were then applied to the amorphous neat PEEK properties given in Table 2 to arrive at consistent semi-crystalline properties. The employed percentage change factors are plotted in Figure 11. Note that Talbott et al. [31] also provided an empirical equation for the shear modulus of neat PEEK as a function of crystallinity, but the use of this equation resulted in unrealistic Poisson's ratios. As such, it was assumed that Poisson's ratio of the neat PEEK remains constant with crystallinity, which, in accordance with isotropy, resulted in the shear modulus changing by the same factor as the Young's modulus. Further, Talbott et al. [31] did not address the effect of crystallinity on CTE, but evidence in the literature [26,32] suggests a much smaller impact compared to that observed on the mechanical properties. As such, it was assumed that the thermal conductivity of the neat PEEK was not affected by the degree of crystallinity.

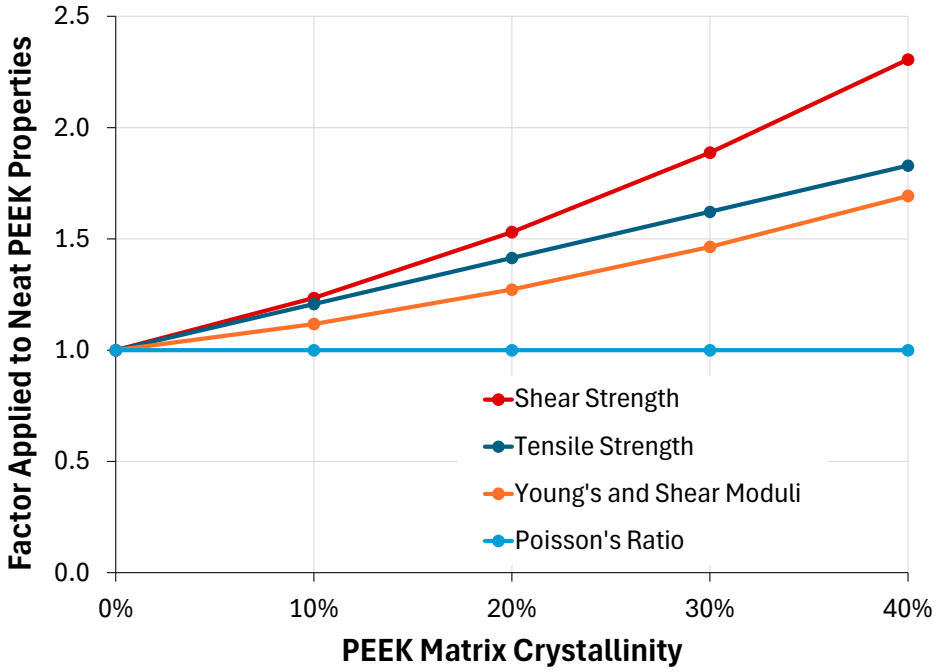

Figure 11. Factors applied to the neat amorphous PEEK properties (Table 2), based on the empirical equations provided by Talbott et al. [31], to approximate the neat PEEK properties as a function of crystallinity.

The predictions of the 0.603 fiber volume fraction unidirectional AS4/PEEK properties are shown in Figure 12, with comparison to test data values from a Trelleborg datasheet [33] and statistical mechanical test data given by Maekawa et al. [34]. These test data are for semi-crystalline PEEK matrix composites and are not a function of the PEEK matrix crystallinity. Rather, they likely represent a typical PEEK crystallinity value of approximately 33% [35]. A range of ±one standard deviation of the data reported by Maekawa et al. [34] is shown. Note also the significant differences in the ordinate ranges in the plots of Figure 12.

Figure 12a,c show that, for the longitudinal (fiber-direction) properties, the model predictions are only weakly influenced by matrix degree of crystallinity (as expected in this fiber-dominated direction). The agreement with test data is good, but it suggests the employed AS4 fiber modulus and strain to failure (Table 1) might be slightly too low. Also, as expected, the predicted transverse Young's modulus and tensile strength (Figure 12b,d) show a strong dependence on the PEEK degree of crystallinity. Further, at realistic PEEK crystallinities (~33%), the predictions agree quite well with the test data, with the predicted transverse Young's modulus slightly underpredicted and the transverse tensile strength slightly overpredicted.

The predicted AS4/PEEK longitudinal CTE is clearly realistic and in range with the (very low) test data in this fiber-dominated direction (Figure 12e). Figure 12f suggests that the transverse CTE might be overpredicted. However, it has been assumed here that the PEEK matrix CTE is not a function of crystallinity, so the transverse CTE is highly dependent on the amorphous CTE value, which is quite high at room temperature (67.7×10^{-6}/°C, see Table 2). In addition, the transverse CTE predicted by the composite is quite dependent on the fiber transverse CTE, which is typically not a well-known property.

While the approach taken here to account for the crystallinity in the model predictions is quite simplistic, these results indicate that the AS4/PEEK model is reasonable and realistic. Figure 12b,d suggest that treating the PEEK matrix as amorphous rather than semi-crystalline has resulted in underpredicting the AS4/PEEK transverse Young's modulus and strength by 23% and 39%, respectively, compared to the mean values reported by Maekawa

et al. [34]. Figure 12f suggests an overprediction of the transverse CTE. These uncertainties would tend to lower the TPC performance as predicted by the model, again pointing to the results herein as lower bounds. As mentioned previously, future work will address this shortcoming by explicitly modeling the crystalline microstructure, starting with MD predictions of the amorphous and crystalline thermoplastic phases.

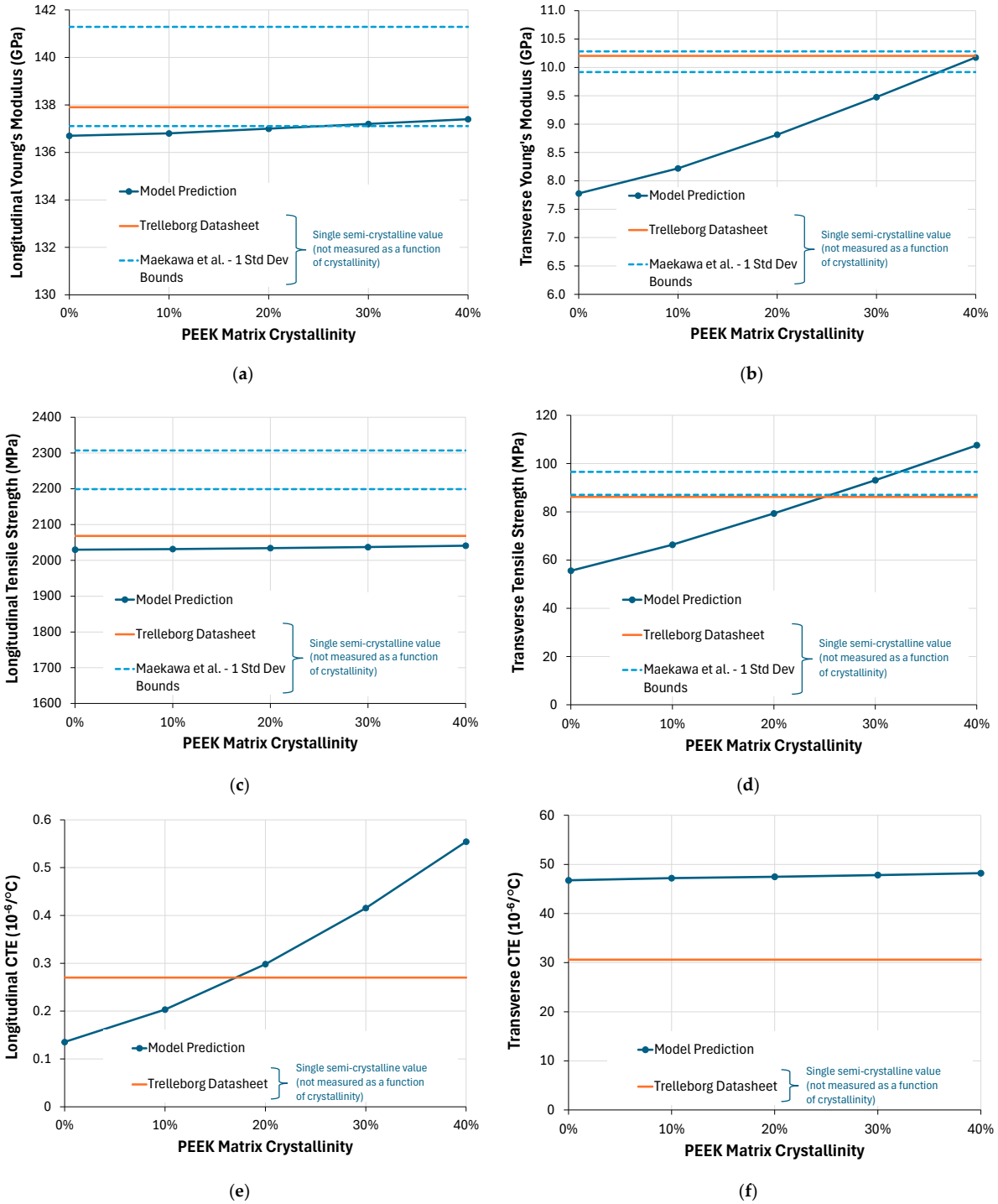

Figure 12. Predicted composite properties for unidirectional AS4/PEEK as a function of crystallinity of the PEEK matrix compared with data from the Trelleborg data sheet [32] and statistics from Maekawa et al. [34]. (**a**) Longitudinal Young's modulus. (**b**) Transverse Young's modulus. (**c**) Longitudinal tensile strength. (**d**) Transverse tensile strength. (**e**) Longitudinal CTE. (**f**) Transverse CTE.

Overall, these results underscore the critical importance of selecting both matrix material and laminate architecture to maximize microcrack resistance, and hence permeability resistance, in thermoplastic composite cryotanks. Of the candidates considered, the Double-Double and $[0/\pm30/\pm60]_s$ layups combined with a high-performance matrix such as LM-PAEK or PEKK offer the most robust performance under representative thermal and mechanical service conditions.

4. Conclusions

This work demonstrates the powerful synergy of molecular-scale simulations and recursive multiscale micromechanics for evaluating thermoplastic matrix composites in hydrogen cryotanks. By feeding temperature-dependent polymer properties from LAMMPS-based MD directly into a NASMAT MsRM model, the buildup of thermal mismatch stresses during cooldown to -253 °C was captured. Then, biaxial mechanical loads, representative of cylindrical cryotank acreage, were applied. Progressive damage simulations across four realistic laminate architectures revealed that microcrack initiation, and thus permeability risk, is clearly influenced by the ratio of matrix yield strength to the thermal stress driver properties ($E \cdot \alpha$). Among the six candidate matrices, LM PAEK and PEKK consistently offered the greatest resistance to early cracking, while PEEK and PEI exhibited microcrack initiation during the thermal cooldown, underscoring the need for both high strength and low thermoelastic mismatch.

Of the architectures examined, the $[55/5/-55/-5]$ Double-Double layup delivered the highest crack-initiation thresholds across all matrices. Final burst predictions, tied to fiber failure, were similar for all combinations, confirming that fiber properties ultimately limit tensile strength, but that matrix performance dictates early-stage damage. These insights highlight that optimal cryotank design requires concurrent selection of both matrix chemistry and ply architecture to suppress microcracking under service loads.

To frame the presented results with respect to real AS4/thermoplastic composites, an empirical method was used to account for crystallinity in the PEEK material so that comparisons could be made to available composite test data in which the matrix is semi-crystalline. Good agreement was demonstrated between test results and this model for unidirectional AS4/PEEK, with the possible exception of the transverse CTE. These results indicated that the employed models are likely realistic but definitely represent lower bounds on the TPC performance quantitatively.

Looking forward, integrating semi-crystalline phase behavior in the MD models and adopting energy-based damage criteria in the multiscale framework would further enhance predictive fidelity. Extending the approach to three-dimensional crack network simulations would also enable direct estimates of permeability. Validation via correlation with additional experimental data is needed as well. Nonetheless, the present methodology offers a robust, fully computational pathway for screening emerging thermoplastics and layups, accelerating the development of safe, leak-resistant, linerless composite cryotanks for next-generation hydrogen propulsion.

Author Contributions: Conceptualization, B.A.B., B.L.H. and E.J.P.; methodology, B.A.B., B.L.H. and E.J.P.; software, B.A.B., B.L.H. and E.J.P.; formal analysis, B.A.B.; investigation, B.A.B., B.L.H. and E.J.P.; data curation, B.L.H.; writing—original draft preparation, B.A.B.; writing—review and editing, B.A.B., B.L.H. and E.J.P.; visualization, B.A.B. and B.L.H. All authors have read and agreed to the published version of the manuscript.

Funding: This research received no external funding.

Data Availability Statement: The dataset is available upon request from the authors.

Acknowledgments: This work was performed at NASA Glenn Research Center under the NASA Aeronautics Mission Directorate CH_2ARGE project, with molecular dynamics data provided by Michigan Technological University and NASA Langley Research Center.

Conflicts of Interest: The authors declare no conflicts of interest.

References

1. Saha, M.C.; Sullivan, R.M. A review on gas permeability of polymer matrix composites for cryogenic applications. *Compos. B Eng.* **2024**, *271*, 111699. [CrossRef]
2. Nachtane, M.; Tarfaoui, M.; Abichou, M.A.; Vetcher, A.; Rouway, M.; Aâmir, A.; Mouadili, H.; Laaouidi, H.; Naanani, H. An Overview of the Recent Advances in Composite Materials and Artificial Intelligence for Hydrogen Storage Vessels Design. *J. Compos. Sci.* **2023**, *7*, 119. [CrossRef]
3. Chen, D.; Li, J.; Yuan, Y.; Gao, C.; Cui, Y.; Li, S.; Liu, X.; Wang, H.; Peng, C.; Wu, Z. A review of the polymer for cryogenic application: Methods, mechanisms and perspectives. *Polymers* **2021**, *13*, 320. [CrossRef]
4. Sápi, Z.; Butler, R. Properties of cryogenic and low temperature composite materials—A review. *Cryogenics* **2020**, *111*, 103190. [CrossRef]
5. Hohe, J.; Neubrand, A.; Fliegener, S.; Beckmann, C.; Schober, M.; Weiss, K.-P.; Appel, S. Performance of fiber reinforced materials under cryogenic conditions—A review. *Compos. A Appl. Sci. Manuf.* **2021**, *141*, 106226. [CrossRef]
6. Wang, C.; Sun, C.T. Thermoelastic behavior of PEEK thermoplastic composite during cooling from forming temperatures. *J. Compos. Mater.* **1997**, *31*, 2230–2248. [CrossRef]
7. Whitley, K.; Gates, T. Thermal/mechanical response and damage growth in polymeric composites at cryogenic temperatures. In Proceedings of the 43rd AIAA/ASME/ASCE/AHS/ASC Structures, Structural Dynamics, and Materials Conference, Denver, CO, USA, 22–25 January 2002. [CrossRef]
8. Grogan, D.M.; Leen, S.B.; Semprimoschnig, C.O.A.; Ó Brádaigh, C.M. Damage characterisation of cryogenically cycled carbon fibre/PEEK laminates. *Compos. A Appl. Sci. Manuf.* **2014**, *66*, 237–250. [CrossRef]
9. Grogan, D.M.; Ó Brádaigh, C.M.; McGarry, J.P.; Leen, S.B. Damage and permeability in tape-laid thermoplastic composite cryogenic tanks. *Compos. A Appl. Sci. Manuf.* **2015**, *78*, 390–402. [CrossRef]
10. Grogan, D.M.; Leen, S.B.; Ó Brádaigh, C.M. An XFEM-based methodology for fatigue delamination and permeability of composites. *Compos. Struct.* **2014**, *107*, 205–218. [CrossRef]
11. Grogan, D.M.; Ó Brádaigh, C.M.; Leen, S.B. A combined XFEM and cohesive zone model for composite laminate microcracking and permeability. *Compos. Struct.* **2015**, *120*, 246–261. [CrossRef]
12. Comer, A.J.; Ray, D.; Obande, W.; McCarthy, M.A. Mechanical characterisation of carbon fibre-PEEK manufactured by laser-assisted automated-tape-placement and autoclave. *Compos. A Appl. Sci. Manuf.* **2015**, *69*, 10–20. [CrossRef]
13. Flanagan, L. Permeability of carbon fibre/PEEK composites for cryogenic storage tanks of future space launchers. *Compos. A Appl. Sci. Manuf.* **2017**, *101*, 173. [CrossRef]
14. Schlothauer, A.; Pappas, G.A.; Ermanni, P. Thin-ply thermoplastic composites: From weak to robust transverse performance through microstructural and morphological tuning. *Compos. B Eng.* **2022**, *261*, 110764. [CrossRef]
15. Nikonovich, M.; Branco, R.G.; Fonseca, A.C.; Ramalho, A.; Emami, N. Structural, thermal, and mechanical characterisation of PEEK-based composites in cryogenic temperature. *Polym. Test.* **2023**, *125*, 108139. [CrossRef]
16. Pourahmadi, E.; Ganeson, R.; Shadmehri, F. Micromechanical characterization of carbon/PEEK thermoplastic composite material in-situ consolidated by automated fiber placement: Stiffness prediction. *Compos. Sci. Technol.* **2024**, *246*, 8. [CrossRef]
17. Wang, Z.; Bailey, W.; Song, J.; Huang, L.; Yang, Y. Evaluating the potential of thermoplastic polymers for cryogenic sealing applications: Strain rate and temperature effects. *arXiv* **2024**. [CrossRef]
18. Roy, S.; Benjamin, M. Modeling of permeation and damage in graphite/epoxy laminates for cryogenic fuel storage. *Compos. Sci. Technol.* **2004**, *64*, 2051–2065. [CrossRef]
19. Nair, A.; Roy, S. Modeling of permeation and damage in graphite/epoxy laminates for cryogenic tanks in the presence of delaminations and stitch cracks. *Compos. Sci. Technol.* **2007**, *67*, 2592–2605. [CrossRef]
20. Sandia National Laboratories. LAMMPS Molecular Dynamics Simulator. Available online: https://www.lammps.org (accessed on 29 September 2025).
21. Soden, P.; Hinton, M.; Kaddour, A. Lamina Properties, lay-up configurations and loading conditions for a range of fibre-reinforced composite laminates. *Compos. Sci. Technol.* **1998**, *58*, 1011–1022. [CrossRef]
22. Tsai, S.W. Double–Double: New Family of Composite Laminates. *AIAA J.* **2021**, *59*, 4293–4305. [CrossRef]
23. Tsai, S.W. *Double-Double a New Perspective on the Manufacture and Design of Composite*; Stanford University: Palo Alto, CA, USA, 2022.

24. Bamane, S.S.; Patil, S.; Kashmari, K.; Jansen, B.; Hinkley, J.; Kang, J.H.; Odegard, G.M. Investigation of material properties of thermoplastic polymer materials at cryogenic temperatures using molecular dynamics. *NASA/TM-20250009461.* **2025**, *in press*.
25. Pisani, W.A.; Radue, W.S.; Chinkanjanarot, S.; Bednarcyk, B.A.; Pineda, E.J.; Waters, K.; Pandey, R.; King, J.A.; Odegard, G.M. Multiscale modeling of PEEK using reactive molecular dynamics modeling and micromechanics. *Polymer* **2019**, *163*, 96–105. [CrossRef]
26. Pineda, E.J.; Husseini, J.F.; Kemppainen, J.D.; Odegard, G.M.; Bednarcyk, B.A.; Pisani, W.A.; Stapleton, S.E. Multiscale modeling of thermoplastics using atomistic-informed micromechanics. *AIAA J.* **2025**, *63*, 2373–2381. [CrossRef]
27. Aboudi, J.; Arnold, S.M.; Bednarcyk, B.A. *Micromechanics of Composite Materials: A Generalized Multiscale Analysis Approach*; Elsevier: Oxford, UK, 2013.
28. Aboudi, J.; Arnold, S.M.; Bednarcyk, B.A. *Practical Micromechanics of Composite Materials*; Elsevier: Oxford, UK, 2021.
29. Pineda, E.J.; Bednarcyk, B.A.; Ricks, T.M.; Arnold, S.M.; Henson, G. Efficient multiscale recursive micromechanics of composites for engineering applications. *Int. J. Multiscale Comput. Eng.* **2021**, *19*, 77–105. [CrossRef]
30. *NASA Multiscale Analysis Tool (NASMAT)*; Version 4.0; National Aeronautics and Space Administration: Washington, DC, USA, 2025. Available online: https://software.nasa.gov/software/LEW-20650-1 (accessed on 29 September 2025).
31. Talbott, M.F.; Springer, G.S.; Berglund, L.A. The effects of crystallinity on the mechanical properties of PEEK polymer and Graphite Fiber Reinforced PEEK. *J. Compos. Mater.* **1987**, *21*, 1056–1081. [CrossRef]
32. Choy, C.L.; Leung, W.P.; Nakafuku, C. Thermal Exapansion of Poly (ether-ether-ketone) (PEEK). *J. Polym. Sci. B Polym. Phys.* **1990**, *28*, 1965–1977. [CrossRef]
33. Trelleborg Group. Continuous AS4 Carbon/PEEK Composite Typical Material Properties. Available online: https://www.trelleborg.com/seals/-/media/tss-media-repository/tss_website/products/advanced-composites/pdf/as4-carbon-peek-data-sheet.pdf? rev=bc2abaced19a4eeeb37e1f2de98d7776, Revision F, 03/03/2008 (accessed on 29 September 2025).
34. Maekawa, Z.; Hamada, H.; Lee, K.; Kitagawa, T. Reliability Evaluation of mechanical properties of AS4/PEEK composites. *Composites* **1994**, *25*, 37–45. [CrossRef]
35. Seo, J.; Gohn, A.M.; Dubin, O.; Takahashi, H.; Hasegawa, H.; Sato, R.; Rhoades, A.M.; Schaake, R.P.; Colby, R.H. Isothermal crystallization of poly(ether ether ketone) with different molecular weights over a wide temperature range. *Polym. Cryst.* **2019**, *2*, e10055. [CrossRef]

Disclaimer/Publisher's Note: The statements, opinions and data contained in all publications are solely those of the individual author(s) and contributor(s) and not of MDPI and/or the editor(s). MDPI and/or the editor(s) disclaim responsibility for any injury to people or property resulting from any ideas, methods, instructions or products referred to in the content.